arXiv:hep-ex/9805025v1 21 May 1998

EUROPEAN LABORATORY FOR PARTICLE PHYSICS

CERN-EP/98-058
30th March 1998

Production of K^0_S and Λ in Quark and Gluon Jets from Z^0 Decay

The OPAL Collaboration

Abstract

The production of K^0_S mesons and Λ baryons in quark and gluon jets has been investigated using two complementary techniques. In the first approach, which provides high statistical accuracy, jets were selected using different jet finding algorithms and ordered according to their energy. Production rates were determined taking into account the dependences of quark and gluon compositions as a function of jet energy as predicted by Monte Carlo models. Selecting three-jet events with the $k_\perp$ (Durham) jet finder ($y_{\rm cut} = 0.005$), the ratios of K^0_S and Λ production rates in gluon and quark jets relative to the mean charged particle multiplicity were found to be $1.10 \pm 0.02 \pm 0.02$ and $1.41 \pm 0.04 \pm 0.04$, respectively, where the first uncertainty is statistical and the second is systematic. In the second approach, a new method of identifying quark jets based on the collimation of energy flow around the jet axis is introduced and was used to anti-tag gluon jets in symmetric (Y-shaped) three-jet events. Using the cone jet finding algorithm with a cone size of 30°, the ratios of relative production rates in gluon and quark jets were determined to be $0.94 \pm 0.07 \pm 0.07$ for K^0_S and $1.18 \pm 0.10 \pm 0.17$ for Λ. The results of both analyses are compared to the predictions of Monte Carlo models.

Submitted to European Physics Journal C.

The OPAL Collaboration

K. Ackerstaff[8], G. Alexander[23], J. Allison[16], N. Altekamp[5], K.J. Anderson[9], S. Anderson[12], S. Arcelli[2], S. Asai[24], S.F. Ashby[1], D. Axen[29], G. Azuelos[18,a], A.H. Ball[17], E. Barberio[8], R.J. Barlow[16], R. Bartoldus[3], J.R. Batley[5], S. Baumann[3], J. Bechtluft[14], T. Behnke[8], K.W. Bell[20], G. Bella[23], S. Bentvelsen[8], S. Bethke[14], S. Betts[15], O. Biebel[14], A. Biguzzi[5], S.D. Bird[16], V. Blobel[27], I.J. Bloodworth[1], M. Bobinski[10], P. Bock[11], J. Böhme[14], M. Boutemeur[34], S. Braibant[8], P. Bright-Thomas[1], R.M. Brown[20], H.J. Burckhart[8], C. Burgard[8], R. Bürgin[10], P. Capiluppi[2], R.K. Carnegie[6], A.A. Carter[13], J.R. Carter[5], C.Y. Chang[17], D.G. Charlton[1,b], D. Chrisman[4], C. Ciocca[2], P.E.L. Clarke[15], E. Clay[15], I. Cohen[23], J.E. Conboy[15], O.C. Cooke[8], C. Couyoumtzelis[13], R.L. Coxe[9], M. Cuffiani[2], S. Dado[22], G.M. Dallavalle[2], R. Davis[30], S. De Jong[12], L.A. del Pozo[4], A. de Roeck[8], K. Desch[8], B. Dienes[33,d], M.S. Dixit[7], M. Doucet[18], J. Dubbert[34], E. Duchovni[26], G. Duckeck[34], I.P. Duerdoth[16], D. Eatough[16], P.G. Estabrooks[6], H.G. Evans[9], F. Fabbri[2], A. Fanfani[2], M. Fanti[2], A.A. Faust[30], F. Fiedler[27], M. Fierro[2], H.M. Fischer[3], I. Fleck[8], R. Folman[26], A. Fürtjes[8], D.I. Futyan[16], P. Gagnon[7], J.W. Gary[4], J. Gascon[18], S.M. Gascon-Shotkin[17], C. Geich-Gimbel[3], T. Geralis[20], G. Giacomelli[2], P. Giacomelli[2], V. Gibson[5], W.R. Gibson[13], D.M. Gingrich[30,a], D. Glenzinski[9], J. Goldberg[22], W. Gorn[4], C. Grandi[2], E. Gross[26], J. Grunhaus[23], M. Gruwé[27], G.G. Hanson[12], M. Hansroul[8], M. Hapke[13], C.K. Hargrove[7], C. Hartmann[3], M. Hauschild[8], C.M. Hawkes[5], R. Hawkings[27], R.J. Hemingway[6], M. Herndon[17], G. Herten[10], R.D. Heuer[8], M.D. Hildreth[8], J.C. Hill[5], S.J. Hillier[1], P.R. Hobson[25], A. Hocker[9], R.J. Homer[1], A.K. Honma[28,a], D. Horváth[32,c], K.R. Hossain[30], R. Howard[29], P. Hüntemeyer[27], P. Igo-Kemenes[11], D.C. Imrie[25], K. Ishii[24], F.R. Jacob[20], A. Jawahery[17], H. Jeremie[18], M. Jimack[1], A. Joly[18], C.R. Jones[5], P. Jovanovic[1], T.R. Junk[8], D. Karlen[6], V. Kartvelishvili[16], K. Kawagoe[24], T. Kawamoto[24], P.I. Kayal[30], R.K. Keeler[28], R.G. Kellogg[17], B.W. Kennedy[20], A. Klier[26], S. Kluth[8], T. Kobayashi[24], M. Kobel[3,e], D.S. Koetke[6], T.P. Kokott[3], M. Kolrep[10], S. Komamiya[24], R.V. Kowalewski[28], T. Kress[11], P. Krieger[6], J. von Krogh[11], P. Kyberd[13], G.D. Lafferty[16], D. Lanske[14], J. Lauber[15], S.R. Lautenschlager[31], I. Lawson[28], J.G. Layter[4], D. Lazic[22], A.M. Lee[31], E. Lefebvre[18], D. Lellouch[26], J. Letts[12], L. Levinson[26], R. Liebisch[11], B. List[8], C. Littlewood[5], A.W. Lloyd[1], S.L. Lloyd[13], F.K. Loebinger[16], G.D. Long[28], M.J. Losty[7], J. Ludwig[10], D. Lui[12], A. Macchiolo[2], A. Macpherson[30], M. Mannelli[8], S. Marcellini[2], C. Markopoulos[13], A.J. Martin[13], J.P. Martin[18], G. Martinez[17], T. Mashimo[24], P. Mättig[26], W.J. McDonald[30], J. McKenna[29], E.A. Mckigney[15], T.J. McMahon[1], R.A. McPherson[28], F. Meijers[8], S. Menke[3], F.S. Merritt[9], H. Mes[7], J. Meyer[27], A. Michelini[2], S. Mihara[24], G. Mikenberg[26], D.J. Miller[15], R. Mir[26], W. Mohr[10], A. Montanari[2], T. Mori[24], K. Nagai[26], I. Nakamura[24], H.A. Neal[12], B. Nellen[3], R. Nisius[8], S.W. O'Neale[1], F.G. Oakham[7], F. Odorici[2], H.O. Ogren[12], M.J. Oreglia[9], S. Orito[24], J. Pálinkás[33,d], G. Pásztor[32], J.R. Pater[16], G.N. Patrick[20], J. Patt[10], R. Perez-Ochoa[8], S. Petzold[27], P. Pfeifenschneider[14], J.E. Pilcher[9], J. Pinfold[30], D.E. Plane[8], P. Poffenberger[28], B. Poli[2], J. Polok[8], M. Przybzien[8], C. Rembser[8], H. Rick[8],

S. Robertson[28], S.A. Robins[22], N. Rodning[30], J.M. Roney[28], K. Roscoe[16], A.M. Rossi[2], Y. Rozen[22], K. Runge[10], O. Runolfsson[8], D.R. Rust[12], K. Sachs[10], T. Saeki[24], O. Sahr[34], W.M. Sang[25], E.K.G. Sarkisyan[23], C. Sbarra[29], A.D. Schaile[34], O. Schaile[34], F. Scharf[3], P. Scharff-Hansen[8], J. Schieck[11], B. Schmitt[8], S. Schmitt[11], A. Schöning[8], T. Schorner[34], M. Schröder[8], M. Schumacher[3], C. Schwick[8], W.G. Scott[20], R. Seuster[14], T.G. Shears[8], B.C. Shen[4], C.H. Shepherd-Themistocleous[8], P. Sherwood[15], G.P. Siroli[2], A. Sittler[27], A. Skuja[17], A.M. Smith[8], G.A. Snow[17], R. Sobie[28], S. Söldner-Rembold[10], M. Sproston[20], A. Stahl[3], K. Stephens[16], J. Steuerer[27], K. Stoll[10], D. Strom[19], R. Ströhmer[34], R. Tafirout[18], S.D. Talbot[1], S. Tanaka[24], P. Taras[18], S. Tarem[22], R. Teuscher[8], M. Thiergen[10], M.A. Thomson[8], E. von Törne[3], E. Torrence[8], S. Towers[6], I. Trigger[18], Z. Trócsányi[33], E. Tsur[23], A.S. Turcot[9], M.F. Turner-Watson[8], R. Van Kooten[12], P. Vannerem[10], M. Verzocchi[10], P. Vikas[18], H. Voss[3], F. Wäckerle[10], A. Wagner[27], C.P. Ward[5], D.R. Ward[5], P.M. Watkins[1], A.T. Watson[1], N.K. Watson[1], P.S. Wells[8], N. Wermes[3], J.S. White[28], G.W. Wilson[14], J.A. Wilson[1], T.R. Wyatt[16], S. Yamashita[24], G. Yekutieli[26], V. Zacek[18], D. Zer-Zion[8]

[1]School of Physics and Astronomy, University of Birmingham, Birmingham B15 2TT, UK
[2]Dipartimento di Fisica dell' Università di Bologna and INFN, I-40126 Bologna, Italy
[3]Physikalisches Institut, Universität Bonn, D-53115 Bonn, Germany
[4]Department of Physics, University of California, Riverside CA 92521, USA
[5]Cavendish Laboratory, Cambridge CB3 0HE, UK
[6]Ottawa-Carleton Institute for Physics, Department of Physics, Carleton University, Ottawa, Ontario K1S 5B6, Canada
[7]Centre for Research in Particle Physics, Carleton University, Ottawa, Ontario K1S 5B6, Canada
[8]CERN, European Organisation for Particle Physics, CH-1211 Geneva 23, Switzerland
[9]Enrico Fermi Institute and Department of Physics, University of Chicago, Chicago IL 60637, USA
[10]Fakultät für Physik, Albert Ludwigs Universität, D-79104 Freiburg, Germany
[11]Physikalisches Institut, Universität Heidelberg, D-69120 Heidelberg, Germany
[12]Indiana University, Department of Physics, Swain Hall West 117, Bloomington IN 47405, USA
[13]Queen Mary and Westfield College, University of London, London E1 4NS, UK
[14]Technische Hochschule Aachen, III Physikalisches Institut, Sommerfeldstrasse 26-28, D-52056 Aachen, Germany
[15]University College London, London WC1E 6BT, UK
[16]Department of Physics, Schuster Laboratory, The University, Manchester M13 9PL, UK
[17]Department of Physics, University of Maryland, College Park, MD 20742, USA
[18]Laboratoire de Physique Nucléaire, Université de Montréal, Montréal, Quebec H3C 3J7, Canada
[19]University of Oregon, Department of Physics, Eugene OR 97403, USA
[20]Rutherford Appleton Laboratory, Chilton, Didcot, Oxfordshire OX11 0QX, UK

[22]Department of Physics, Technion-Israel Institute of Technology, Haifa 32000, Israel
[23]Department of Physics and Astronomy, Tel Aviv University, Tel Aviv 69978, Israel
[24]International Centre for Elementary Particle Physics and Department of Physics, University of Tokyo, Tokyo 113, and Kobe University, Kobe 657, Japan
[25]Institute of Physical and Environmental Sciences, Brunel University, Uxbridge, Middlesex UB8 3PH, UK
[26]Particle Physics Department, Weizmann Institute of Science, Rehovot 76100, Israel
[27]Universität Hamburg/DESY, II Institut für Experimental Physik, Notkestrasse 85, D-22607 Hamburg, Germany
[28]University of Victoria, Department of Physics, P O Box 3055, Victoria BC V8W 3P6, Canada
[29]University of British Columbia, Department of Physics, Vancouver BC V6T 1Z1, Canada
[30]University of Alberta, Department of Physics, Edmonton AB T6G 2J1, Canada
[31]Duke University, Dept of Physics, Durham, NC 27708-0305, USA
[32]Research Institute for Particle and Nuclear Physics, H-1525 Budapest, P O Box 49, Hungary
[33]Institute of Nuclear Research, H-4001 Debrecen, P O Box 51, Hungary
[34]Ludwigs-Maximilians-Universität München, Sektion Physik, Am Coulombwall 1, D-85748 Garching, Germany

[a] and at TRIUMF, Vancouver, Canada V6T 2A3
[b] and Royal Society University Research Fellow
[c] and Institute of Nuclear Research, Debrecen, Hungary
[d] and Department of Experimental Physics, Lajos Kossuth University, Debrecen, Hungary
[e] on leave of absence from the University of Freiburg

1 Introduction

In recent years, clear differences between quark and gluon jets have been established experimentally [1–6]. These studies have mostly exploited the large samples of Z^0 decay events recorded at the CERN LEP collider, and have examined three-jet events with a symmetric event topology favouring the direct comparison of quark and gluon jets of the same energy produced in the same event topology. In particular, gluon jets have been measured to have a larger mean particle multiplicity, a softer fragmentation function and a larger angular width than quark jets of the same energy. Comparisons between jets produced in e^+e^- and $p\overline{p}$ collisions also indicate that gluon jets are broader than quark jets [7]. This is in qualitative agreement with the predictions of perturbative QCD [8]. Perturbative QCD makes no explicit predictions for the individual hadron species produced in these jets, but some QCD Monte Carlo models of hadronization predict that the relative hadron production rates in quark and gluon jets differ for different hadron species.

Few experimental results are available on the production of identified particles in quark and gluon jets. Results from e^+e^- annihilations at center-of-mass (c.m.) energies around the $\Upsilon(1S)$ resonance (≈ 10 GeV) indicate that baryons are produced about 2.5 times more copiously in direct $\Upsilon(1S)$ decays ($\Upsilon(1S) \to ggg \to$ hadrons) than in continuum events ($e^+e^- \to q\overline{q} \to$ hadrons) whilst no such enhancement was observed for mesons [9]. An OPAL investigation [10] studied identified particle production in jet topologies enriched in gluon and quark jets and found no jet-dependent differences in the production of mesons and charged particles (other than protons). In contrast, baryons were found to be produced more copiously in gluon-enriched jet samples. The DELPHI collaboration has reported measurements of $K^{\pm}$, K^0, p and Λ in secondary-vertex tagged quark and gluon jets in symmetric (Y-shaped) events [11]. Within relatively large statistical and systematic uncertainties, they find the ratio of identified particle rates in quark and gluon jets to be consistent with that for charged particles. Recently, L3 has concluded that production of K^0 and Λ in both quark and gluon jets is well modelled by string fragmentation [12].

In this paper an experimental comparison of K^0 and Λ production in quark and gluon jets is presented. Two complementary analyses of data recorded with the OPAL detector at LEP are presented, using different approaches to identify quark and gluon jets. One analysis separates quark and gluon jets according to their energies, giving a large sample of events, whilst the other selects a smaller sample of tagged quark and gluon jets in symmetric (Y-shaped) events, which allows for a simpler interpretation, but with larger uncertainties.

In the first analysis (the 'energy-based analysis') the production of K^0_S mesons and Λ baryons[1] in quark and gluon jets was investigated in three-jet events of different topologies selected with the $k_\perp$ (Durham) [13] or a cone [7] jet finder. The jets were ordered by their energy since the lowest energy jets are mainly induced by gluons, and higher energy jets mainly by quarks. Motivated by Monte Carlo investigations a similar energy dependence for the production rates of all hadron species was assumed, and the production rates of K^0_S

[1]For simplicity Λ refers to both Λ and $\overline{\Lambda}$.

and Λ relative to those of charged particles were determined. The experimental relative rates were corrected for the underlying mixture of quark and gluon jets, allowing the K^0_S and Λ relative production rates in pure quark and gluon jets to be obtained.

In the second analysis (the 'Y-event analysis'), a comparison was made of the absolute production rates of K^0_S mesons and Λ baryons in quark and gluon jets produced under the same conditions, embedded in similar event topologies. Symmetric three-jet events were analysed, where the two lower energy jets (assumed to be initiated by a quark and a gluon) were produced at about 150° with respect to the higher energy jet. A sample of anti-tagged gluon jets containing about 30% of the symmetric event sample was isolated by means of a new method of identifying the quark jets based on the observation that light quark jets are more collimated than gluon jets [3]. The inclusive yield of charged particles in these jets was also measured, allowing relative rates to be evaluated. The production rates of the particles in the lower energy jets of the inclusive symmetric sample were determined, and a correction applied in order to obtain measurements corresponding to pure samples of quark and gluon jets.

Section 2 gives a description of the main features of the OPAL detector, of the data and simulated event samples and of the reconstruction algorithms for K^0_S and Λ. Section 3 describes the details of the energy-based analysis, and section 4 the Y-event analysis. The results of both analyses are presented and discussed in section 5, before the summary is given in section 6.

2 The OPAL Detector and Data Samples

2.1 The OPAL Detector

The OPAL detector is described in detail elsewhere [14]. Of most relevance for the present analyses are the tracking system and the electromagnetic calorimeter. The tracking system consists of a silicon microvertex detector, an inner vertex chamber, a large-volume jet chamber and specialised chambers at the outer radius of the jet chamber which improve the measurements in the z direction[2] (z-chambers). The tracking system covers the region $|\cos\theta| < 0.95$ and is enclosed by a solenoidal magnet coil with an axial field of 0.435 T. The tracking detectors provide momentum measurements of charged particles, and particle identification from measurements of the ionisation energy loss, $\mathrm{d}E/\mathrm{d}x$. Electromagnetic energy is measured by a lead-glass calorimeter located outside the magnet coil, which covers $|\cos\theta| < 0.98$.

2.2 Data Samples

The energy-based analysis, which is not statistics limited, used 2.8 million events recorded between 1992 and 1994 whilst the Y-event analysis used the full OPAL data sample of

[2]The coordinate system is defined so that z is the coordinate parallel to the e^- beam axis, r is the coordinate normal to the beam axis, ϕ is the azimuthal angle around the beam axis and θ is the polar angle with respect to z.

about 4.2 million hadronic events collected around the Z^0 peak from 1990 to 1995. The procedures for identifying hadronic events using measurements of tracks and electromagnetic energy are described in [15]. The criteria applied to select tracks and deposits of electromagnetic energy (clusters) for the analyses were identical to those in [3]. Each accepted track and unassociated electromagnetic cluster was considered to be a particle. Tracks were assigned the pion mass and electromagnetic clusters were assigned zero mass since they originate mostly from photons.

To reduce background from non-hadronic decays of the Z^0 and to eliminate events in which a significant number of particles were lost near the beam direction, both analyses required that $|\cos(\theta_{\rm thrust})| < 0.9$ ($\theta_{\rm thrust}$ is the polar angle of the thrust axis); also, there had to be at least five accepted tracks. The residual background from all sources was estimated to be less than 1%. In addition, for the energy-based analysis, events were rejected if they contained tracks with measured momentum greater than 60 GeV/c, if the absolute value of the vector sum of all selected particles $|\vec{p}_{\rm tot}|$ exceeded 30 GeV/c, or if the visible energy (the sum of the energies of all the accepted tracks and clusters) was less than 40% of the center-of-mass energy.

2.3 Reconstruction of K^0_S and Λ

The neutral strange K^0_S mesons and Λ baryons were reconstructed by their decay channels $K^0_S \to \pi^+\pi^-$ and $\Lambda \to \pi^-$p. The reconstruction algorithms, signal definitions, efficiency corrections and background subtractions are all described in [16] and [17]. Briefly, tracks of opposite charge were paired and regarded as a secondary vertex candidate if at least one track pair intersection in the plane perpendicular to the beam axis satisfied the criteria of a neutral two-body decay with the appropriate lifetime. Each track pair passing these requirements was refitted with the constraint that the tracks originated from a common vertex, and background from photon conversions was suppressed. For Λ candidates, information from dE/dx measurements was used to help identify the π and p for further background suppression. Two sets of cuts are described in [17] for Λ identification.[3] For the energy-based analysis, Λ candidates were reconstructed using method 1, which is optimized to have good mass and momentum resolution, while in the Y-event analysis the more efficient method 2 was employed to maximize the number of Λ candidates.

Candidates for K^0_S with momentum greater than 0.150 GeV/c and with an invariant mass in the range 0.3 GeV/c^2 $< m_{\pi\pi} <$ 0.8 GeV/c^2 and Λ candidates with momentum greater than 0.520 GeV/c and with an invariant mass in the range 1.08 GeV/c^2 $m_{\pi p} <$ 1.2 GeV/c^2 were retained for further analysis. The K^0_S rates were determined by fitting the mass spectrum with a third-order polynomial excluding a signal region of $\pm$0.05 GeV/c^2 around the nominal mass. The shape of the background under the Λ signal was fitted using a function of the form $(1 - e^{-a(\mathrm{m}_{\pi p} - 1.077)}) \times (b \cdot \mathrm{m}_{\pi p} + c)$, excluding a signal window of $\pm$0.012 GeV/c^2 around the nominal Λ mass. For each particle species the entries in the signal region were summed and the background as determined by the fit was subtracted. The efficiency of the identification algorithms was determined as a function of candidate

[3] The two sets of cuts are described as 'method 1' and 'method 2' in [17].

momentum from Monte Carlo events, and subsequently used to correct the number of observed signal events.

For the energy-based analysis, candidates for Λ and K^0_S were formed and then supplied to the jet finder, whereas this order was reversed in the case of the Y-events. Monte Carlo studies showed that for the Y-event analysis there is no systematic effect due to the order of jet finding and particle reconstruction.

2.4 Monte Carlo Event Samples

Samples of Monte Carlo hadronic events with a full simulation of the OPAL detector [18] and including initial state photon radiation were used to evaluate the detector acceptance and resolution, and to study the efficiency and purity of the quark and gluon jet identification and the particle reconstruction algorithms. In total, 7 million simulated events were available, of which 4 million were generated by JETSET 7.4 [19] with fragmentation parameters described in [4], and 3 million generated by JETSET 7.3 with fragmentation parameters described in [2]. The JETSET 7.4 events included updated particle decay tables and heavy meson resonances and were processed using a more recent version of the detector simulation compared to the JETSET 7.3 sample. It should be noted that there are significant differences in the simulation of baryon production between the two JETSET samples.

For comparison with the experimental results, the Monte Carlo models JETSET 7.4 and HERWIG 5.9[4] [20] were used. The models both give a good description of global event shapes and many inclusive particle production rates, but differ in their description of the perturbative phase and their implementation of the hadronization mechanism.

Tracks and clusters were selected in the Monte Carlo events, which include detector simulation, in the same way as for the data: the resulting four-vectors of particles are referred to as being at the 'detector level'. Alternatively, Monte Carlo samples without initial-state photon radiation or detector simulation were used, with all charged and neutral particles with mean lifetimes greater than $3 \cdot 10^{-10}$ s treated as stable. The four-vectors of the resulting particles are referred to as being at 'generator level'. The remaining quarks and gluons after the termination of the parton shower in these events are referred to as being at the 'parton level'.

3 The Energy-Based Analysis

3.1 Selection of Three-Jet Events

Two different types of algorithms are commonly used for jet definition: recombination jet finders and cone jet finders. The treatment of high momentum particles which lie close to

[4]The fragmentation parameters of HERWIG 5.9 were identical to those used by the OPAL tuned version of HERWIG 5.8 [21] with the exception of the parameter `CLMAX` which was set to 3.75 in order to improve the description of the mean charged particle multiplicity value in inclusive hadronic Z^0 decays.

the jet axes is similar for both types of jet finder, but there are substantial differences in the assignment to the jets of soft particles far from the jet axes. Recombination algorithms combine all particles into jets, whereas cone finders do not associate particles outside the cones. The recombination jet finders iteratively combine pairs of particles until the scaled resolution parameter (y) of all subsequent pairings exceeds the jet resolution parameter $y_{\rm cut}$. The cone jet finder associates particles into jets that lie within a cone of fixed half-angle R. The cone axis is determined from the vector sum of the momenta of the particles contained therein.

To illustrate the sensitivity of the analysis to event topology and jet reconstruction algorithm, we selected three samples of three-jet events with different average topologies, using either the $k_\perp$ jet finding algorithm [13], or the cone algorithm [7]. The main selection, containing the largest number of three-jet events, was obtained using the $k_\perp$ algorithm with a resolution parameter, $y_{\rm cut} = 0.005$. The second sample of three-jet events ($y_{\rm win}$ sample) was selected from a window of y-values between 0.008 and 0.016, i.e., the event should be classified as three-jet for some value of $y_{\rm cut}$ within this window. Monte Carlo studies at the generator and parton level showed that hadronization effects on the angles of jets selected in this sample are small. The average resolution parameter $y_{\rm cut}$ for these events to be clustered into three jets was about 0.01. Finally, a third sample of three-jet events was selected using the cone jet finder with the parameters $R = 0.7$ rad and $\varepsilon = 7$ GeV, where ε is the minimum energy contained in the jet cone. These parameters were chosen to give a good correspondence between jets reconstructed at the generator and parton levels in Monte Carlo events [7].

Both jet finding algorithms were applied using reconstructed $\rm K^0_S$ and Λ candidates, accepted charged tracks (excluding the decay products of $\rm K^0_S$ and Λ) and the electromagnetic clusters not associated to tracks. Additional quality cuts were then applied to the selected three-jet events. Each jet was required to contain at least two charged tracks, to have more than 5 GeV of visible energy and to lie in the polar region $|\cos\theta| < 0.9$. The sum of the angles between all three jets had to exceed 358° to eliminate non-planar events, and the angle between the two lower energy jets was required to be larger than 30°. Finally, the jets in each event were each assigned a calculated energy based on the measured jet directions and assuming massless kinematics.

After all cuts, 24.0% of events were selected by the $y_{\rm cut}$ selection, 18.1% by the $y_{\rm win}$ selection, and 15.5% by the cone selection. The tighter selection criteria for the $y_{\rm win}$ and the cone samples, yielding a lower number of three-jet events, were partly compensated by an improved reconstruction quality e.g., a better agreement of the jets at the parton and generator level. In total, samples of about 500,000 three-jet events were retained for further analysis. In figure 1 the energy spectra of the jets in the $y_{\rm cut}$ sample is shown. The jet energy distributions are more peaked in the $y_{\rm cut}$ selection compared to the $y_{\rm win}$ and cone selections. The relatively small number of events containing a jet with energy below 7.5 GeV ($\approx 15\%$) were excluded from further analysis.

In general, the angular separation of the jets (jet topology), is dependent on the event selection. In particular, the $y_{\rm cut}$ selection gave the most collimated sample of events, with an average angle between the two lowest energy jets of about 62°. This can be compared

to average angles of about 70° for the $y_{\rm win}$ sample and about 76° for the cone selection.

3.2 Determination of Jet Purities

Since the jets selected in any given energy interval were a mixture of quark and gluon jets, JETSET Monte Carlo events were used to determine the quark and gluon jet content of the samples in the following manner. The Monte Carlo events were selected in the same way as the data events and were accepted if classified as three-jet events at detector level. From the partons of these events exactly three jets were reconstructed. The detector level jets closest in angle to the parton level jets containing the primary quark and anti-quark were considered to be the quark jets and the remaining jet the gluon jet. The term quark (gluon) 'jet purity' is defined to be the fraction of jets in a given energy bin, initiated by quarks (gluons). The purities of the jets as a function of jet energy are shown in figure 2. The lowest energy jet samples contained in excess of 85% gluons, whereas the high energy samples were composed of over 95% quark jets. The purity distributions as a function of jet energy determined with the $k_\perp$ algorithm in the $y_{\rm cut}$ and $y_{\rm win}$ samples agree to within 1%. The gluon jet purity in the cone sample was lower than that of the $y_{\rm cut}$ and $y_{\rm win}$ samples by a few percent in very low and in high energy jets. The HERWIG Monte Carlo model and JETSET in matrix element mode [19] predict similar jet purities to the standard JETSET samples, and detector effects on the purity distribution were found to be small.

3.3 Determination of Particle Rates

With the $y_{\rm cut}$ selection, about 100,000 $\rm K^0_S$ and about 30,000 Λ were reconstructed. The production rates per jet of charged particles, $\rm K^0_S$ mesons and Λ baryons in jets, $n_{\rm ch}$, $n_{\rm K^0_S}$, and n_Λ, are shown as functions of the jet energy in figure 3 after corrections for reconstruction efficiency (about 16%) and detector acceptance. The decay products of $\rm K^0_S$ and Λ were not counted as charged particles. The predictions of the JETSET 7.4 and HERWIG 5.9 Monte Carlo models are also shown in figure 3. Whereas the JETSET 7.4 generator describes the experimental data fairly well, the predictions of HERWIG 5.9 agree poorly with the data. Similar results were obtained with the three-jet events from the $y_{\rm win}$ and the cone selections.

3.4 Relative Rates and Correction for Jet Impurity

The particle production rates rise with the jet energy partly due to the changing mixture of gluon and quark jets, and partly due to the increased energy available for particle production. In order to measure differences due to quark and gluon jets, it is necessary to remove this jet energy dependence. If a similar energy dependence for the production rates of all hadron species is assumed, then the relative particle production rate (defined as the rate of $\rm K^0_S$ or Λ production divided by the rate of charged particle production, $R_{\rm K^0_S} = n_{\rm K^0_S}/n_{\rm ch}$ and $R_\Lambda = n_\Lambda/n_{\rm ch}$) would be independent of the jet energy. Studies

of JETSET events showed that there is indeed only a weak energy dependence of these relative production rates in pure quark and gluon jets, figure 4. The lines are fits of straight lines and have slopes smaller than 2×10^{-4} GeV^{-1}. For gluon jets the slopes are smaller than for quark jets, and for K^0_S smaller than for Λ. As JETSET gives a good overall description of the data over a large range of c.m. and jet energies, it was assumed for further analysis that the relative particle production rates are constant in the data and we choose this assumption to reduce the dependence on Monte Carlo models. The consistency of the results with this assumption will be shown later. Particle production in jets depends not only on the jet energy but also on the proximity of the other jets in the event [22]. Further Monte Carlo studies showed that this angular dependence is almost the same for all hadron species and does not affect the relative rates.

The relative particle production rates of K^0_S and Λ were computed in each jet energy interval from the ratios of the rates shown in figure 3. The relative rates for pure quark and gluon jets were unfolded using the jet purities for each three-jet event sample, obtained from Monte Carlo results shown in figure 2. A fit was performed to the observed relative rates as a function of jet energy E_j using the function:

$$R^h_m(E_j) = R^h_g \cdot \rho_g(E_j) + R^h_q \cdot (1 - \rho_g(E_j)), \tag{1}$$

where $R^h_m(E_j)$ is the measured relative particle rate, $\rho_g(E_j)$ the gluon purity of the jets, and R^h_q and R^h_g the relative rates in pure quark and gluon jets, with $h = K^0_S, \Lambda$ (h = hadron). R^h_q and R^h_g were assumed to be constant for the reasons stated above.

The fit was performed in the jet energy range from 7.5 GeV to 45.0 GeV. The relative particle rates as a function of the jet energy are shown in figure 5 for the $y_{\rm cut}$ selection, with the lines giving the fit results. The fit results and χ^2/d.o.f. values for all three selections are given in table 1. In order to compare particle production in quark and gluon jets, the ratios $(R_g/R_q)_\Lambda$ and $(R_g/R_q)_{\rm K}$ were studied. These are given in table 2 and will be discussed fully in section 5.

3.5 Systematic Uncertainties

The following sources of systematic uncertainty on the measured ratios of relative rates have been studied. For each source of uncertainty, the difference with respect to the standard analysis was used to estimate a symmetric systematic uncertainty. The uncertainties listed in table 3 were added in quadrature to arrive at a total systematic error.

Three-jet event reconstruction: The analysis was repeated with the following changes:

- charged tracks only were used for the reconstruction of jets, instead of charged tracks and unassociated electromagnetic clusters. This check disregards all calorimeter information when determining energy flows in the events, so the changes represent an extreme situation. A systematic error was therefore determined from the difference divided by $\sqrt{12}/2$ (= 1.7);

- the resolution parameter of the $k_\perp$ jet-finder was varied by replacing the $y_{\rm cut}$ = 0.005 selection by selecting three-jet events in a window of y-values (0.004, 0.008). The $y_{\rm win}$ selection was modified by requiring a cut at a fixed value, $y_{\rm cut}$ = 0.01.

Λ and K^0_S reconstruction: As in [16] and [17] the major sources of systematic uncertainties for the reconstruction of K^0_S and Λ were found to be the background determination and the reliability of the Monte Carlo simulation for distributions on which cuts were placed.

- The K^0_S and Λ selection criteria were varied as in [16] and [17]. In particular, the cut on the distance between the reconstructed secondary vertex and the first measured hit of the decay particles was loosened from 3 to 9 cm;
- a sideband method [17] was applied to determine the backgrounds under the K^0_S and Λ signals; and
- systematic uncertainties on the strange particle reconstruction efficiencies were estimated by calculating the efficiencies separately using the JETSET 7.3 and JETSET 7.4 samples (the standard analysis used the combined JETSET 7.3 and 7.4 samples). The simulation of baryon production differs considerably in these samples and they were taken to represent alternative possibilities of generator tuning and detector simulation. Studies of events generated using HERWIG as input to the detector simulation gave efficiencies lying in the range spanned by JETSET 7.3 and JETSET 7.4. A symmetric systematic uncertainty was assigned using the full difference between JETSET 7.3 and JETSET 7.4 divided by $\sqrt{12}$.

Quark and gluon jet unfolding: The systematic uncertainties in the determination of K^0_S and Λ production in quark and gluon jets were obtained by the following variations:

- the upper and lower bounds of the fit range ($7.5 - 45.0$ GeV) were changed to 12.5 and 40 GeV respectively;
- the influence of the jet purity determination was studied by varying the purities by their systematic uncertainties (about 5%), which were derived as described in [23]. Briefly, the uncertainty in the identification of quark and gluon jets was estimated by comparing different fragmentation models (JETSET and HERWIG) and studying detector resolution effects;
- as a check of the fit procedure, the relative production rates in pure gluon jets were obtained by a linear fit to the relative rates $n_m(\rho_g)$ as a function of the gluon jet purity ρ_g above $\rho_g \geq 8\%$, and extrapolating to 100% gluon jet purity;
- the fit function was modified to account for a possible linear energy dependence of the relative particle production rates in pure quark and gluon jets, using the JETSET slopes as shown in figure 4. It can be seen from table 3 that

considering non-zero values of the slopes results in only a small contribution to the systematic uncertainties. This means that the relative rates found in the experimental data are consistent with the assumption of independence of the jet energy.

The main contributions to the systematic uncertainties came from the variation of the cuts on K^0_S and Λ candidates, from the differences in detection efficiencies determined using JETSET 7.3 and JETSET 7.4, and from the variation of the fit ranges. The ratios of relative rates determined from the fit were essentially unchanged if contributions from K^0_S and Λ decay products were included in the charged particle rates.

Finally, Monte Carlo events with full detector simulation were analysed in the same manner as the data. The relative rates derived from the fits (0.95 ± 0.02 for K^0_S and 1.27 ± 0.04 for Λ) were compared with those determined directly at the generator level in these events (0.94 and 1.26 respectively). The agreement for both Λ and K^0_S from the $y_{\rm cut}$ sample is good. The results from the other two jet samples agreed equally well.

4 The Y-event Analysis

4.1 Three-jet Event Selection

For the Y-event analysis, jets were defined with the cone jet finding algorithm, supplying all accepted particles as input. The resolution parameters chosen for the jet finder were a cone size $R = 30^\circ$, as in an earlier publication [4], and a minimum jet energy ε computed once for each event according to $\varepsilon = 5 \times E_{\rm vis}/\sqrt{s}$ GeV where $\sqrt{s}$ is the c.m. energy and $E_{\rm vis}$ the sum of the energy of the particles.

The criteria given in references [1–4] were followed to select a sample of symmetric three-jet events. Each jet was required to contain at least two particles and to lie in the polar angle region $|\cos\theta| < 0.9$, and the sum of the angles between the three jets was required to exceed 358°. As in the energy-based approach, the jets in each event were assigned a calculated energy based on the interjet angles, assuming massless kinematics. Strongly symmetric three-jet events were selected by projecting the jets into the three-jet event plane and requiring the angles between the jet with the highest calculated energy and each of the two others to be in the range $150^\circ \pm 10^\circ$. The event plane is defined as the plane perpendicular to the sphericity [24] eigenvector associated with the smallest eigenvalue. In total, 70,738 symmetric three-jet events were found. The mean calculated jet energies were 42.50 ± 0.01 GeV for the highest energy jet and 24.37 ± 0.01 GeV for the two lower energy jets. The highest energy jets are likely to be quark jets with high probability, due to the nature of the gluon radiation spectrum. From a Monte Carlo study, this probability was estimated to be 97.3%. The two lower energy jets were therefore assumed to be a quark jet and a gluon jet of equal energy with the same angles with respect to the other two jets in the event. The inclusive sample of lower energy jets is referred to as the 'normal-mixture' sample of jets.

4.2 Gluon Jet Identification

A gluon-jet enriched sample of the lower energy jets was selected by a new variant of the method [1–4] of identifying quark jets in order to 'anti-tag' the gluon jets. For each lower energy jet identified as a quark jet, the other lower energy jet was assumed to be a gluon jet. This anti-tagged sample of gluon jets was therefore essentially unbiased by the tagging method. It contained a well known fraction of gluon jets established from studies of simulated events.

Previous studies employed the reconstruction of secondary vertices or the identification of energetic leptons to identify jets that originated from heavy quarks. Whilst this yielded an anti-tagged jet sample with a gluon purity typically in excess of 90%, the efficiency to identify quark jets was only of order 5%. The present analysis introduces a new method to isolate a large sample of quark jets by identifying jets that are collimated, i.e. that have a large fraction of their energy close to the jet axis. Studies of quark and gluon jets in symmetric events have shown that gluon jets are broader than quark jets [3] and this is well reproduced by Monte Carlo models.

In particular, the quantity f_Θ is determined, which is given by the fraction of the jet's energy contained in a cone co-axial with the jet axis and with half-angle Θ. If the energy of the particles contained in the sub-cone is E_Θ and the visible jet energy is $E_{\rm jet}$ then $f_\Theta = \frac{E_\Theta}{E_{\rm jet}}$. The f_Θ distributions were studied in detector level Monte Carlo events. Three-jet events were selected as above, and f_Θ determined for the two lower energy jets. Each simulated hadron jet was associated with an underlying quark or gluon jet using the method described in [3]. Briefly, the two hadron jets that were closest in angle to the directions of the primary quark and anti-quark which had evolved from the Z^0 decay were considered to be the quark jets, and the remaining jet was identified as the gluon jet. Figure 6 shows the distributions of f_Θ for $\Theta = 7^\circ$ for jets in the simulated events that were classified as quark or gluon jets. The quark jets tend to have larger f_Θ values than the gluon jets, and a sample of jets with a high quark content can therefore be selected by requiring f_Θ to exceed some threshold $f_\Theta^{\rm cut}$, – for example $f_\Theta^{\rm cut} = 0.75$.

The anti-tagged jet purity $\rho_{\rm g}$ is defined to be the fraction of anti-tagged jets that are indeed associated with an underlying gluon jet, and the tagging rate, $\mathcal{P}_{\rm tag}$, is defined to be the fraction of normal-mixture Y-events which contain jets that are anti-tagged. From Monte Carlo studies, the normal-mixture sample of jets had a gluon content, $\rho_{\rm n.mix} = 48.7 \pm 0.2\%$. The anti-tagged jet purity and the tag rate depend on the values of Θ and $f_\Theta^{\rm cut}$, and values of $\rho_{\rm g}$ of up to about 80% can be achieved whilst maintaining a tag rate in excess of about 30%. A high gluon purity is desirable for the algebraic correction procedure later, and therefore $\Theta = 7^\circ$ and $f_\Theta^{\rm cut} = 0.75$ were chosen for the standard tag. From studies of Monte Carlo events the values $\mathcal{P}_{\rm tag} = 30.3 \pm 0.2\%$ and $\rho_{\rm g} = 77.0 \pm 0.5 \pm 0.9\%$ were determined, where the first error is statistical and the second systematic. The systematic error includes contributions from the choice of Monte Carlo model (JETSET 7.4, JETSET 7.3 or HERWIG 5.9) and the method used to identify the quark jet in the simulated events (the method described in section 3.2 for the energy-based analysis was used as an alternative). In the data, $\Theta = 7^\circ$ and $f_\Theta^{\rm cut} = 0.75$ gave a tag rate of $31.0 \pm 0.2\%$ (23,256

anti-tagged jets) which is well described by the simulated events. The average energy of the anti-tagged jets was 23.59 ± 0.02 GeV.

In about 1.9% of events both of the lower energy jets fulfilled the tag criteria due to misidentification of collimated gluon jets (the highest energy jet is the gluon in fewer than 10% of these cases), and therefore in these events both the lower energy jets were included in the anti-tagged gluon jet sample. The double tag rate rose to about 3.5% for $\Theta = 8^\circ$ and $f_\Theta^{\rm cut} = 0.75$.

The flavour composition of the tagged, anti-tagged and normal-mixture jets in the Monte Carlo events is shown in table 4. Significantly fewer b-flavour jets were tagged than light-flavour jets which is consistent with the observation that b quark jets in Z^0 decays are broader than light quark jets [4]; a small reduction is also visible in the rate of tagging c-flavour jets. The light quark flavour composition of the tagged jets reflects the relative couplings of u- and d-type quarks to the Z^0. There is a fairly good correspondence between the quark flavour properties of the normal-mixture and anti-tagged jet samples. It was shown in [3] that there is no significant systematic bias to the measurements of quark and gluon jet differences from the flavour composition of the anti-tagged jets. The flavour composition of the quark jets in the anti-tagged sample is therefore not expected to give a systematic bias in the present analysis.

4.3 Correction Methods

Strange Particle Identification

K^0_S mesons and Λ baryons were reconstructed as described in section 2.3. Their invariant mass spectra were computed in bins of momentum, $p_{K^0_s}$ and p_Λ, within the normal-mixture and anti-tagged jets separately. A K^0_S or a Λ candidate was assigned to a jet if its momentum vector fell within the cone defining the jet, i.e., if it lay less than 30° from the jet axis. If a K^0_S or Λ was within 30° of both jets, it was assigned to the higher (calculated) energy jet.

The detection efficiencies of the K^0_S and Λ finding algorithms were sensitive to the particle momenta and to the track environment, and were therefore determined from simulated events for each bin of $p_{K^0_s}$ and p_Λ within the normal-mixture and anti-tagged jets separately. The efficiency was computed from the fraction of generated K^0_S or Λ within a jet that were found in the same jet by the algorithm. The background-subtracted numbers of K^0_S and Λ were corrected for detection efficiency as a function of momentum, and summed to give the production rates of K^0_S and Λ in normal-mixture and anti-tagged jets, $D^{K^0_S}_{\rm n.mix}$ and $D^{K^0_S}_{\rm a.tag}$, $D^{\Lambda}_{\rm n.mix}$ and $D^{\Lambda}_{\rm a.tag}$.

Algebraic Correction Procedure

The algebraic method introduced in [2] was used to correct for quark and gluon misidentification and to arrive at the ratio of the identified particle production rates for pure quark and gluon jets.

The production rate of particle type i in the normal-mixture sample of jets, $D^i_{\rm n.mix}$ may be written

$$D^i_{\rm n.mix} = \rho_{\rm n.mix} \cdot G^i \ + \ (1 - \rho_{\rm n.mix}) \cdot Q^i \quad , \tag{2}$$

where G^i and Q^i are the production rates of i in pure gluon and quark jets respectively. Similarly, the production rate in the anti-tagged sample $D^i_{\rm a.tag}$ may be written

$$D^i_{\rm a.tag} = \rho_{\rm g} \cdot G^i \ + \ (1 - \rho_{\rm g}) \cdot Q^i \quad . \tag{3}$$

The ratio of the production rates for pure gluon and quark jets $\mathcal{R}^i_{\rm gq}$ may therefore be determined by

$$\mathcal{R}^i_{\rm gq} = \frac{G^i}{Q^i} = \frac{(1 - \rho_{\rm n.mix}) \cdot (D^i_{\rm a.tag}/D^i_{\rm n.mix}) - (1 - \rho_{\rm g})}{\rho_{\rm g} - \rho_{\rm n.mix}(D^i_{\rm a.tag}/D^i_{\rm n.mix})} \quad . \tag{4}$$

As in the case of the multiplicity measurement in [4] it was assumed for the purposes of the algebraic correction that Q^i and G^i are the same in equations 2 and 3. This is a reasonable assumption, as the quark flavour compositions of the normal-mixture and anti-tagged samples are generally consistent, and as the properties of energetic acolinear gluons are independent of event flavour according to QCD. The simulated events provide a good representation of the relevant event properties such as the collimation of jets. Therefore any residual effects are expected to be removed by the corrections for detector effects.

The measured production rates D^i appear in equation 4 as the ratio $(D^i_{\rm a.tag}/D^i_{\rm n.mix})$ and therefore some systematic effects related to particle identification are expected to cancel. Statistical uncertainties on $\mathcal{R}^i_{\rm gq}$ were estimated from the variance of the results obtained when the analysis was repeated ten times with the data split into independent subsets. This procedure correctly takes into account correlations between $D^i_{\rm a.tag}$ and $D^i_{\rm n.mix}$.

Detector Corrections

A correction derived from Monte Carlo events was applied to correct for detector acceptance and resolution. The correction was formed from the ratio of $\mathcal{R}^i_{\rm gq}$ values determined at the generator and detector levels. At the generator level, the same three-jet event selection criteria as for the data were applied (with the exception of the requirement $|\cos\theta| < 0.9$ for the jet axes). Monte Carlo information was used to identify quark and gluon jets, as well as particle type. The detector corrections were determined to be 1.105 ± 0.005 for charged particles, 1.023 ± 0.006 for $\rm K^0_S$ and 1.058 ± 0.008 for Λ with uncertainties due to the limited statistics of the Monte Carlo samples. The correction factor for charged particles agrees well with that determined in [3]. The final results can be found in table 6 which will be discussed later.

4.4 Systematic Uncertainties

Systematic uncertainties, which are listed in table 5, were evaluated from a number of sources in a similar fashion to the energy-based analysis described in section 3.5. The total systematic errors were obtained by combining the individual contributions in quadrature.

Detector effects: The total energy and momentum flow in the event were estimated using charged tracks only instead of tracks and electromagnetic clusters. These were used as input to the jet finding and quark jet identification algorithms and the analysis was repeated. The observed jets are more collimated when measured using tracking information only. This is reproduced by the Monte Carlo, both at the generator and detector levels and is partly due to decays of π^0 into photons which tend to broaden the flow of neutral particles in the jet. The effect of this increased collimation was that the anti-tagged jet purities and tag rates were somewhat different to the standard case, with $\rho_{\rm g} = 70.2 \pm 0.4\%$ and $\mathcal{P}_{\rm tag} = 42.0 \pm 0.2\%$ for $\Theta = 7^\circ$ and $f_\Theta^{\rm cut} = 0.75$. The uncertainty was estimated from the difference divided by $\sqrt{12}/2$ as for the energy-based analysis above.

Quark jet identification: The analysis was repeated using parameters $\Theta = 8^\circ$ and $f_\Theta^{\rm cut} = 0.75$ since its tagging rate ($\mathcal{P}_{\rm tag} = 40.1 \pm 0.2$), and the anti-tagged jet purity ($\rho_{\rm g} = 74.7 \pm 0.4 \pm 0.9$) were somewhat different compared to the standard analysis.

Event selection: Events were selected requiring a minimum jet energy of 10 GeV which is the selection criterion used in [3].

Jet purity determination: A number of sources of systematic uncertainty on $\rho_{\rm g}$ have been considered. Simulated events from the JETSET 7.4 and JETSET 7.3 samples were used separately to determine the purities and tag rates, and the observed differences were used to evaluate an uncertainty related to the event generator tuning and detector simulation. A further uncertainty comes from the ambiguity in defining whether a jet arises from a quark or a gluon, as described in a previous OPAL publication [4]. The same procedures were followed to determine a systematic error which was added in quadrature with the other sources to arrive at the total systematic uncertainty. The analysis was repeated using the tagged and normal-mixture jet purity values varied by their combined statistical and systematic uncertainties.

Background determination: The fit ranges, signal window sizes and excluded regions were all varied to determine the background to the selected $\rm K^0_S$ and Λ signals. In the case of the Λ an alternative function was also used to describe the background. Finally a sideband method was used to determine the background.

Efficiency determination: The JETSET 7.3 and JETSET 7.4 samples of simulated events were used separately to estimate the efficiency of the $\rm K^0_S$ and Λ finding algorithms. The two Monte Carlo samples are taken to represent alternative possibilities of generator tuning and detector simulation and an uncertainty was estimated as for the energy-based analysis above. Several of the systematic variations were made simultaneously, and in no case was a difference larger than that for JETSET 7.3 observed.

Monte Carlo statistics: The finite numbers of simulated events available led to statistical uncertainties in the particle detection efficiencies, and the detector corrections.

The effect of varying the cone size R that defines the jets has been investigated in [3] where an increase in $\mathcal{R}_{\rm gq}^{\rm ch}$ with R was observed. Other sources of uncertainty such as changing the requirement on the angle between the highest energy and the other jets, and modifying the track and cluster selection criteria have been considered in that publication and found to be negligible. There were also no statistically significant differences between the detector acceptance corrections computed with the JETSET 7.3 or JETSET 7.4 samples.

5 Results and Discussion

The results of the energy-based analysis are given in table 2. The ratios $R_g^{\rm K^0_S}/R_q^{\rm K^0_S}$ and $R_g^{\Lambda}/R_q^{\Lambda}$ of relative $\rm K^0_S$ and Λ production rates in pure gluon and quark jets are given for all three event selections, together with their statistical and systematic uncertainties and the predictions of the JETSET 7.4 model. For the $y_{\rm cut}$ selection, the production of $\rm K^0_S$ mesons is enhanced in gluon jets relative to quark jets by a factor $1.10 \pm 0.02 \pm 0.02$ where the first error is statistical and the second systematic. Similar results were obtained with the other event selections. The relative production rate of Λ baryons was found to be increased in gluon jets relative to quark jets by $1.41 \pm 0.04 \pm 0.04$ in the $y_{\rm cut}$ selection. The less collimated $y_{\rm win}$ and cone event samples show a smaller increase in the relative production rates of Λ baryons indicating a possible dependence of the baryon production rates on the topology of the events.

For the Y-event analysis, the ratios of absolute production rates of $\rm K^0_S$ and Λ in 24 GeV gluon and quark jets were found to be $\mathcal{R}_{\rm gq}^{\rm K^0_s} = 1.05 \pm 0.08 \pm 0.09$ and $\mathcal{R}_{\rm gq}^{\Lambda} = 1.32 \pm 0.11 \pm 0.18$ for jets defined with the cone algorithm using a cone size of 30°. The corresponding result for charged particles is $\mathcal{R}_{\rm gq}^{\rm ch} = 1.116 \pm 0.006 \pm 0.012$ which is in good agreement with the result from the previous OPAL vertex-tagged analysis ($1.10 \pm 0.02 \pm 0.02$ [3]) and which has a reduced statistical error as a result of the use of the more efficient energy flow tag.

The measurements in the Y-event analysis may also be used to determine production rates of $\rm K^0_S$ and Λ in quark and gluon jets relative to those of charged particles. The relative rates of $\rm K^0_S$ and Λ production are $R_g^{\rm K^0_S}/R_q^{\rm K^0_S} = 0.94 \pm 0.07 \pm 0.07$ and $R_g^{\Lambda}/R_q^{\Lambda} = 1.18 \pm 0.10 \pm 0.17$, where correlations between the sources of systematic uncertainty (given in table 5) have been taken into account.

An enhancement of Λ production in gluon jets relative to quark jets, in excess of that observed for charged particles, is measured by both analyses, with the ratios of the relative Λ rates consistent within the errors. The ratios of the relative production rates of $\rm K^0_S$ mesons in gluon and quark jets are also compatible within the errors, and suggest a small enhancement relative to charged particles. The analyses presented here are consistent with previous findings [3, 22] that have shown that factors such as jet finder, jet energy and event topology are important in quantifying the differences between quark and gluon jets. Therefore, care should be taken to ensure that the conditions are equivalent when comparing results between experiments.

The measurements of relative production rates in gluon and quark jets from both analyses are shown in figure 7 together with the predictions of the JETSET 7.4 and HER-

WIG 5.9 Monte Carlo models. These data are also given in table 6 together with the measurements of absolute rates from the Y-event analysis. HERWIG 5.9, despite its good description of global event properties, fails to give an adequate description of the measurements of ratios of strange particle production rates in quark and gluon jets. This result is not surprising given the poor description of the inclusive strange particle rates as a function of jet energy shown in figure 3. JETSET 7.4, however, was shown to provide a reasonable general description of the data in figure 3, and the ratios of relative rates from the Y-event sample are consistent with its predictions for both K^0_S and Λ. The ratios of relative rates from the energy-based analysis, however, are significantly larger than those predicted for both K^0_S and Λ. The predictions of the ratios of relative production rates from JETSET 7.3 differ from JETSET 7.4 by at most 0.04 which gives an indication of the size of possible effects due to parameter tuning and inclusion of additional particle decay channels.

There is no perturbative mechanism in the JETSET model that gives rise to the observed differences in particle production between quark and gluon jets; they arise from the effects of hadronization and particle decays. Many of the K^0_S are the decay products of heavy (b and c flavour) hadrons. As the production of b and c quarks in gluon jets is suppressed, there are correspondingly fewer K^0_S in these jets. The enhancement of Λ production (and of baryons in general) in gluon jets relative to quark jets predicted by JETSET is a consequence of the different dynamics of the string fragmentation process in quark and gluon jets.

6 Summary

Production rates for K^0_S and Λ have been measured in quark and gluon jets from Z^0 decays with two complementary approaches. In the first analysis a procedure was introduced to compare particle production in gluon and quark jets of different energies facilitating the study of up to about 24% of the total event sample. Different jet finding algorithms ($k_\perp$, cone) were used to investigate samples with different three-jet event topologies. Relative rates, normalized to the inclusive charged particle rate, were obtained for pure quark and gluon jets considering the different quark and gluon content of jets in different energy intervals. The relative rates in pure gluon and quark jets were found to be consistent with being independent of the jet energies, and to depend slightly on the specific jet selection.

In the second analysis a new method was introduced to tag quark jets based on the collimation of their energy flow, allowing the isolation of a larger sample of anti-tagged gluon jets in symmetric three-jet events than the method of secondary vertex tagging used previously. The comparison of quark and gluon jets of equal energies and embedded in almost identical event environments allows for a simple interpretation of the results. The jets were selected using a cone algorithm. By also measuring the inclusive particle rates in these symmetric jets, relative rates were obtained in addition to the absolute rates.

An enhancement of Λ production in gluon jets relative to quark jets, in excess of that for charged particles is observed. The ratios of production rates of K^0_S mesons in gluon and

quark jets suggest a small enhancement relative to charged particles. The results of both analyses are compatible within their errors. The predictions of JETSET 7.4 are consistent with the enhancement observed for Λ, but are smaller for the K^0_S, whilst HERWIG fails to provide an adequate description of the data.

Acknowledgements

We particularly wish to thank the SL Division for the efficient operation of the LEP accelerator at all energies and for their continuing close cooperation with our experimental group. We thank our colleagues from CEA, DAPNIA/SPP, CE-Saclay for their efforts over the years on the time-of-flight and trigger systems which we continue to use. In addition to the support staff at our own institutions we are pleased to acknowledge the
Department of Energy, USA,
National Science Foundation, USA,
Particle Physics and Astronomy Research Council, UK,
Natural Sciences and Engineering Research Council, Canada,
Israel Science Foundation, administered by the Israel Academy of Science and Humanities,
Minerva Gesellschaft,
Benoziyo Center for High Energy Physics,
Japanese Ministry of Education, Science and Culture (the Monbusho) and a grant under the Monbusho International Science Research Program,
German Israeli Bi-national Science Foundation (GIF),
Bundesministerium für Bildung, Wissenschaft, Forschung und Technologie, Germany,
National Research Council of Canada,
Research Corporation, USA,
Hungarian Foundation for Scientific Research, OTKA T-016660, T023793 and OTKA F-023259.

References

[1] OPAL Collaboration, G. Alexander et al., Phys. Lett. **B 265** (1991) 462.

[2] OPAL Collaboration, P. Acton et al., Z. Phys. **C 58** (1993) 387.

[3] OPAL Collaboration, R. Akers et al., Z. Phys. **C 68** (1995) 179.

[4] OPAL Collaboration, G. Alexander et al., Z. Phys. **C 69** (1996) 543.

[5] OPAL Collaboration, G. Alexander et al., Phys. Lett. **B 388** (1996) 659.

[6] ALEPH Collaboration, D. Buskulic et al., Phys. Lett. **B 346** (1995) 389;
DELPHI Collaboration, P. Abreu et al., Z. Phys. **C 70** (1996) 179;
ALEPH Collaboration, D. Buskulic et al., Phys. Lett. **B 384** (1996) 353.

[7] OPAL Collaboration, R. Akers et al., Z. Phys. **C 63** (1994) 197.

[8] S.J. Brodsky and J. Gunion, Phys. Rev. Lett. **37** (1976) 402;
M.B. Einhorn and B.G. Weeks, Nucl. Phys. **B146** (1978) 445.

[9] ARGUS Collaboration, H. Albrecht et al., Phys. Rept. **276** (1996) 223;
CLEO Collaboration, M. S. Alam et al., Phys. Rev. **D 31** (1985) 2161.

[10] Peter Fath, Ph. D. thesis, Universität Heidelberg, Germany 1996 (unpublished).

[11] DELPHI Collaboration, P. Abreu et al., Z. Phys. **C 67** (1995) 543;
DELPHI Collaboration, P. Abreu et al., Phys. Lett. **B 401** (1997) 118.

[12] L3 Collaboration, M. Acciarri et al., Phys. Lett. **B 407** (1997) 389.

[13] S. Catani et al., Phys. Lett. **B 269** (1991) 432;
N. Brown and W.J. Stirling, Z. Phys. **C 53** (1992) 629.

[14] OPAL Collaboration, K. Ahmet et al., Nucl. Instr. and Meth. **A 305** (1991) 275;
P. Allport et al., Nucl. Instrum. Methods **A 346** (1994) 476;
O. Biebel et al., Nucl. Instrum. Methods. **A 323** (1992) 169;
M. Hauschild et al., Nucl. Instrum. Methods. **A 314** (1992) 74.

[15] OPAL Collaboration, G. Alexander et al., Z. Phys. **C 52** (1991) 175.

[16] OPAL Collaboration, R. Akers et al., Z. Phys. **C 67** (1995) 389.

[17] OPAL Collaboration, G. Alexander et al., Z. Phys. **C 73** (1997) 569.

[18] J. Allison et al., Nucl. Instrum. Methods **A 317** (1992) 47.

[19] T. Sjőstrand, Comp. Phys. Comm. **82** (1994) 74.

[20] G. Marchesini, et al., Comp. Phys. Comm. **67** (1992) 465.

[21] OPAL Collaboration, G. Alexander et al., Z. Phys. **C 71** (1996) 191.

[22] Aleph Collaboration, R. Barate et al., Z. Phys. **C 76** (1997) 191.

[23] B. Stockhausen, PhD Thesis, University of Bonn, April 1997 (unpublished).

[24] J.D. Bjorken and S.J. Brodsky, Phys. Rev. **D1** (1970) 1416;
SLAC-LBL Collaboration, G. Hanson et al., Phys. Rev. Lett. **35** (1975) 1609.

Tables

Energy-based	$R_g^{\mathrm{K}^0_{\mathrm{S}}}$	$R_q^{\mathrm{K}^0_{\mathrm{S}}}$	χ^2/d.o.f.
y_{cut}	0.0573 ± 0.0009	0.0522 ± 0.0006	9/13
y_{win}	0.0568 ± 0.0009	0.0531 ± 0.0006	8/13
cone	0.0622 ± 0.0011	0.0580 ± 0.0007	14/13
Energy-based	R_g^{Λ}	R_q^{Λ}	χ^2/d.o.f.
y_{cut}	0.0252 ± 0.0005	0.0179 ± 0.0003	15/13
y_{win}	0.0252 ± 0.0005	0.0188 ± 0.0003	12/13
cone	0.0281 ± 0.0006	0.0214 ± 0.0004	39/13

Table 1: Fitted relative $\mathrm{K}^0_{\mathrm{S}}$ and Λ production rates in gluon and quark jets from the different event selections of the energy-based analysis. The results have been obtained by a fit to equation 1; the fit quality is indicated by the χ^2/d.o.f. values. The errors are statistical.

Energy-based	$R_g^{\mathrm{K}^0_{\mathrm{S}}}/R_q^{\mathrm{K}^0_{\mathrm{S}}}$	JETSET 7.4
y_{cut}	$1.10 \pm 0.02 \pm 0.02$	0.94
y_{win}	$1.07 \pm 0.02 \pm 0.02$	0.94
cone	$1.07 \pm 0.02 \pm 0.02$	0.95
Energy-based	$R_g^{\Lambda}/R_q^{\Lambda}$	JETSET 7.4
y_{cut}	$1.41 \pm 0.04 \pm 0.04$	1.26
y_{win}	$1.34 \pm 0.04 \pm 0.03$	1.24
cone	$1.31 \pm 0.04 \pm 0.05$	1.30

Table 2: Ratios of the relative $\mathrm{K}^0_{\mathrm{S}}$ and Λ production rates in gluon and quark jets from the different event selections of the energy-based analysis compared to the JETSET 7.4 predictions. The first error is statistical and the second systematic.

Source of error	K^0_S			Λ		
Statistical error	2.1 %	2.3 %	2.3 %	2.7 %	3.0 %	3.2 %
Charged tracks only		0.1 %			0.4 %	
$y_{\rm cut}/y_{\rm win}$ change		0.2 %			0.2 %	
Λ/K^0_S cut variation		1.1 %			1.7 %	
Sideband fit		0.6 %			0.1 %	
JETSET 7.3/7.4		0.4 %			0.9 %	
Fit range	0.7 %	0.7 %	0.9 %	1.4 %	0.5 %	1.4 %
Jet purities	0.3 %	0.3 %	0.4 %	0.8 %	0.4 %	0.5 %
Fit method	0.6 %	0.7 %	0.5 %	0.7 %	0.8 %	2.2 %
MC slopes	0.3 %	0.2 %	0.8 %	0.7 %	0.7 %	1.2 %
Total systematic error	1.7 %	1.8 %	2.0 %	2.7 %	2.3 %	3.5 %

Table 3: Statistical and systematic errors of the ratios of relative particle production rates in gluon and quark jets in the energy-based analysis. The three numbers in a row refer to the $y_{\rm cut}$, $y_{\rm win}$, and cone selection.

	Anti-tagged	Tagged	Normal-mixture
d	5.1 ± 0.1	22.1 ± 0.2	11.3 ± 0.1
u	4.2 ± 0.1	18.4 ± 0.2	9.1 ± 0.1
s	5.2 ± 0.1	23.4 ± 0.2	11.4 ± 0.1
c	4.2 ± 0.1	12.8 ± 0.1	9.0 ± 0.1
b	4.2 ± 0.1	4.3 ± 0.1	10.5 ± 0.1
gluon	77.0 ± 0.5	19.0 ± 0.2	48.7 ± 0.2

Table 4: Flavour composition (in %), in the Y-event analysis, of the anti-tagged, tagged and normal-mixture jet samples determined from the JETSET Monte Carlo including simulation of the detector. The quark jet tagging used the parameters $\theta = 7^\circ$ and $f_\Theta^{\rm cut} = 0.75$. The errors are statistical only.

Y-events	Absolute rates			Relative rates	
	$\mathcal{R}_{gq}^{ch}$	$\mathcal{R}_{gq}^{K_s^0}$	$\mathcal{R}_{gq}^{\Lambda}$	K_S^0	Λ
Detector effects	0.003	< 0.01	0.04	< 0.01	0.04
Quark jet identification	0.002	0.05	0.07	0.04	0.06
Event selection	0.010	0.03	0.08	0.02	0.08
Jet purity determination	0.003	< 0.01	0.03	< 0.01	0.01
Background determination	–	0.04	0.05	0.04	0.05
Efficiency determination	< 0.001	0.04	0.11	0.04	0.10
Monte Carlo statistics	0.005	0.03	0.07	0.03	0.07
Total systematic error	0.012	0.09	0.18	0.07	0.17
Statistical error	0.006	0.08	0.11	0.07	0.10

Table 5: Breakdown of the contributions to the uncertainties on the ratios of particle production in quark and gluon jets from the Y-event analysis.

Ratios of relative rates		OPAL Data	JETSET 7.4	HERWIG 5.9
Energy-based	K_S^0	$1.10 \pm 0.02 \pm 0.02$	0.94	0.73
(y_{cut})	Λ	$1.41 \pm 0.04 \pm 0.04$	1.26	0.88
Y-events	K_S^0	$0.94 \pm 0.07 \pm 0.07$	0.95	0.62
	Λ	$1.18 \pm 0.10 \pm 0.17$	1.34	0.87
Ratios of absolute rates		**OPAL Data**	**JETSET 7.4**	**HERWIG 5.9**
Y-events	K_S^0	$1.05 \pm 0.08 \pm 0.08$	1.06	0.70
	Λ	$1.32 \pm 0.11 \pm 0.18$	1.56	0.99
	charged	$1.116 \pm 0.006 \pm 0.012$	1.16	1.13

Table 6: Ratios of the relative K_S^0 and Λ production rates in gluon and quark jets from both analyses, together with the predictions of JETSET 7.4 (the predictions of JETSET 7.3 correspond to those of JETSET 7.4 for K_S^0 and are about 0.04 lower for Λ) and HERWIG 5.9. The ratios of absolute rates determined in the Y-events analysis are also shown.

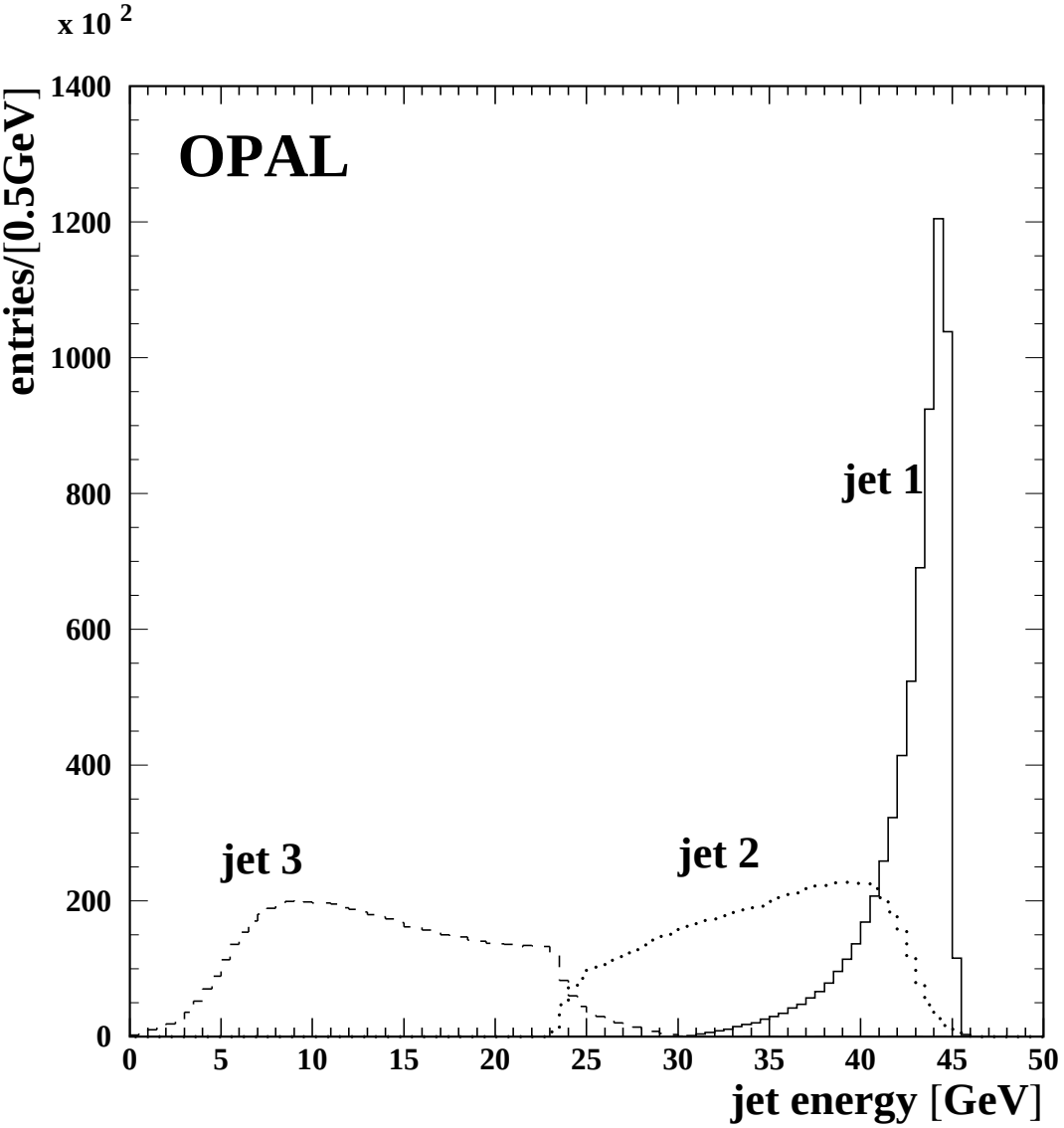

Figure 1: Jet energy distributions of three-jet events selected with the $k_\perp$ jet finder with the $y_{\rm cut}$ event selection.The jets are ordered according to their assigned energies.

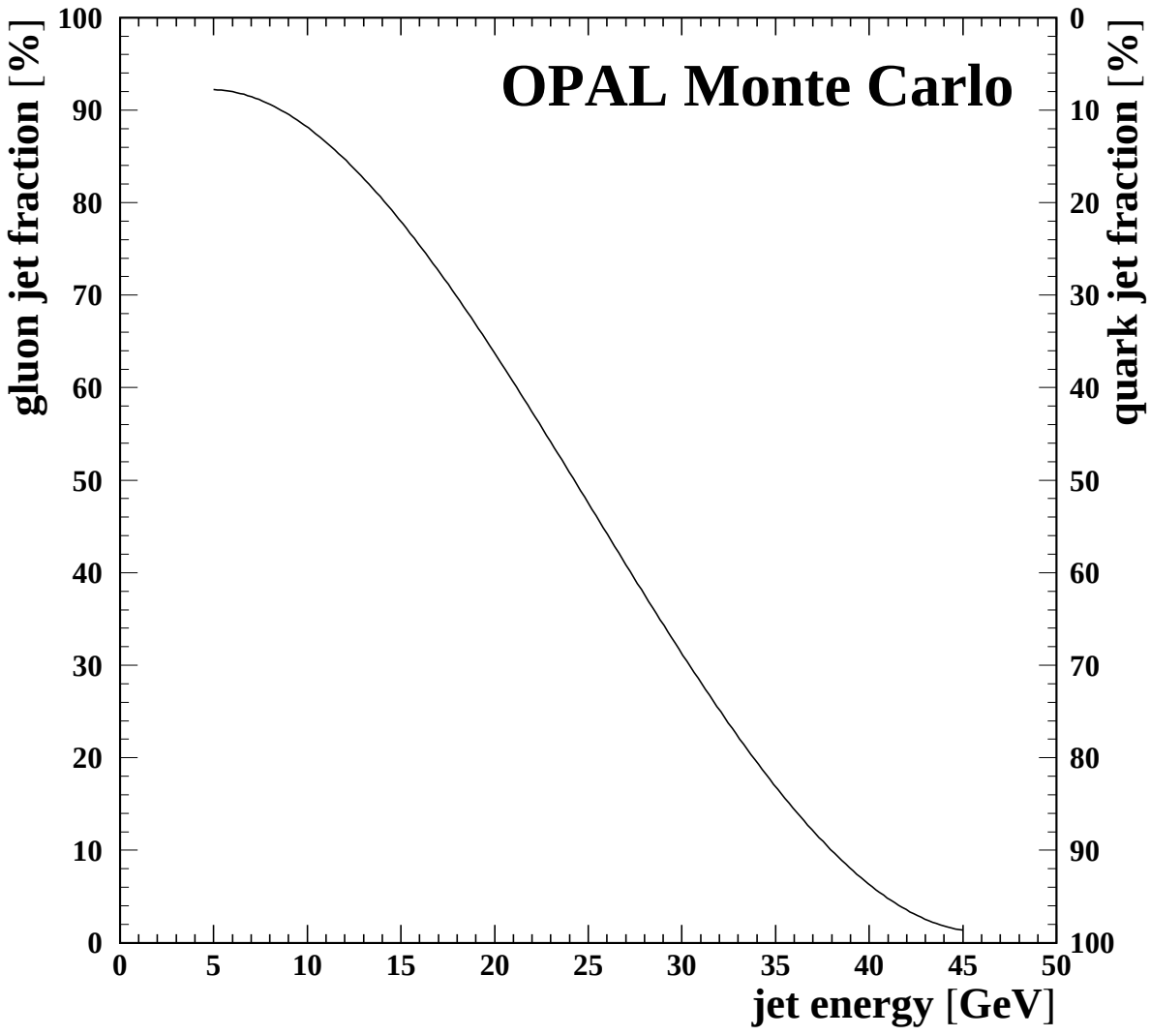

Figure 2: Purities of the reconstructed jets in Monte Carlo events for the $y_{\rm cut}$ event sample.

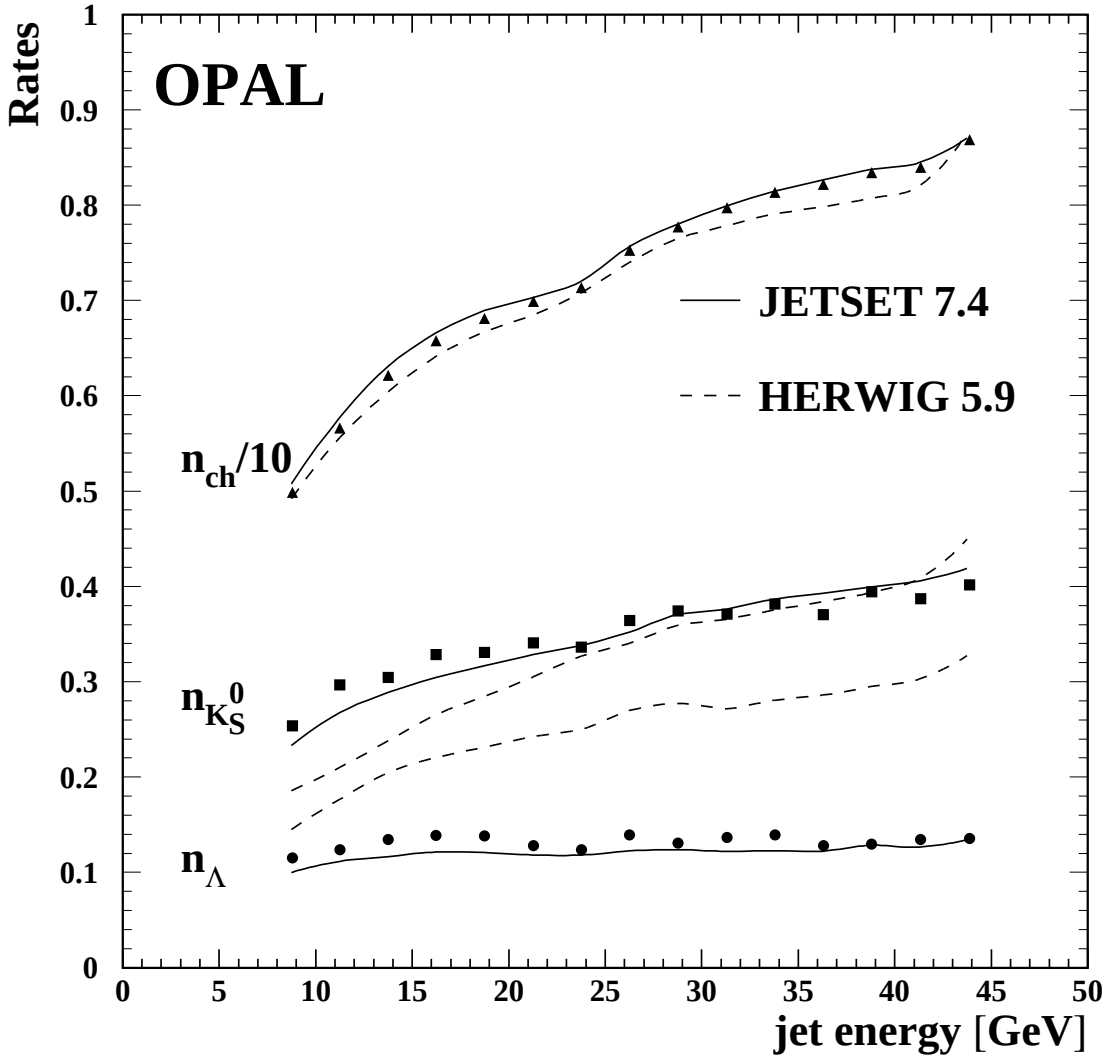

Figure 3: Production rates per jet of charged particles, K_S^0 mesons, and Λ baryons, $n_{ch}/10$, $n_{K_S^0}$, and n_Λ, from the $y_{\rm cut}$ sample as a function of the jet energy compared with the predictions of the models JETSET 7.4 and HERWIG 5.9. The charged particle rates are scaled down by a factor of 10. The errors shown are the (uncorrelated) statistical ones and are mostly smaller than the size of the symbols.

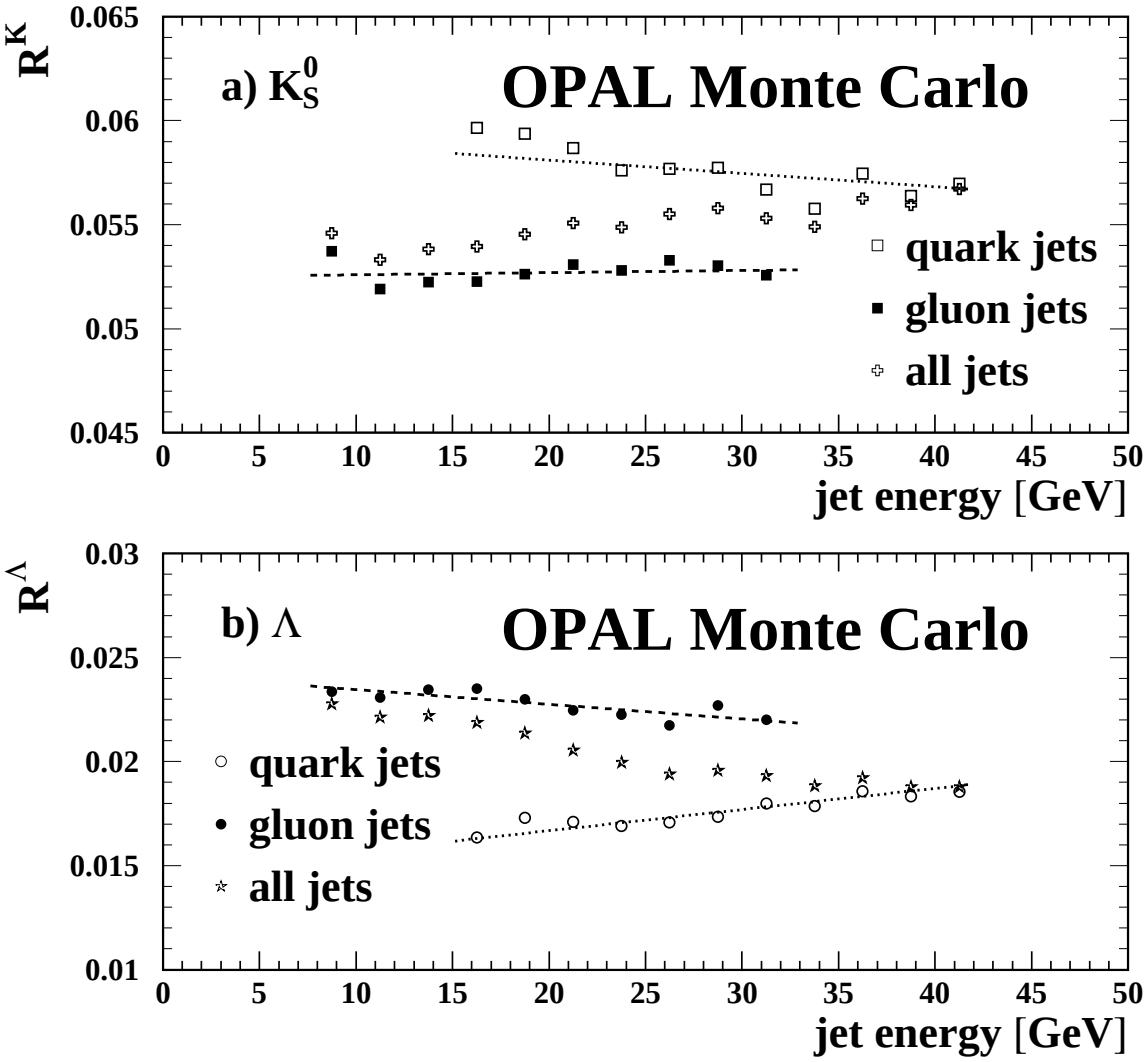

Figure 4: Relative production rates of (a) K^0_S and (b) Λ in JETSET 7.4 events for pure quark and gluon jets as a function of the jet energy. The lines are fits of straight lines to the points. The statistical errors are smaller than the size of the symbols. The zeros of the vertical axes have been suppressed.

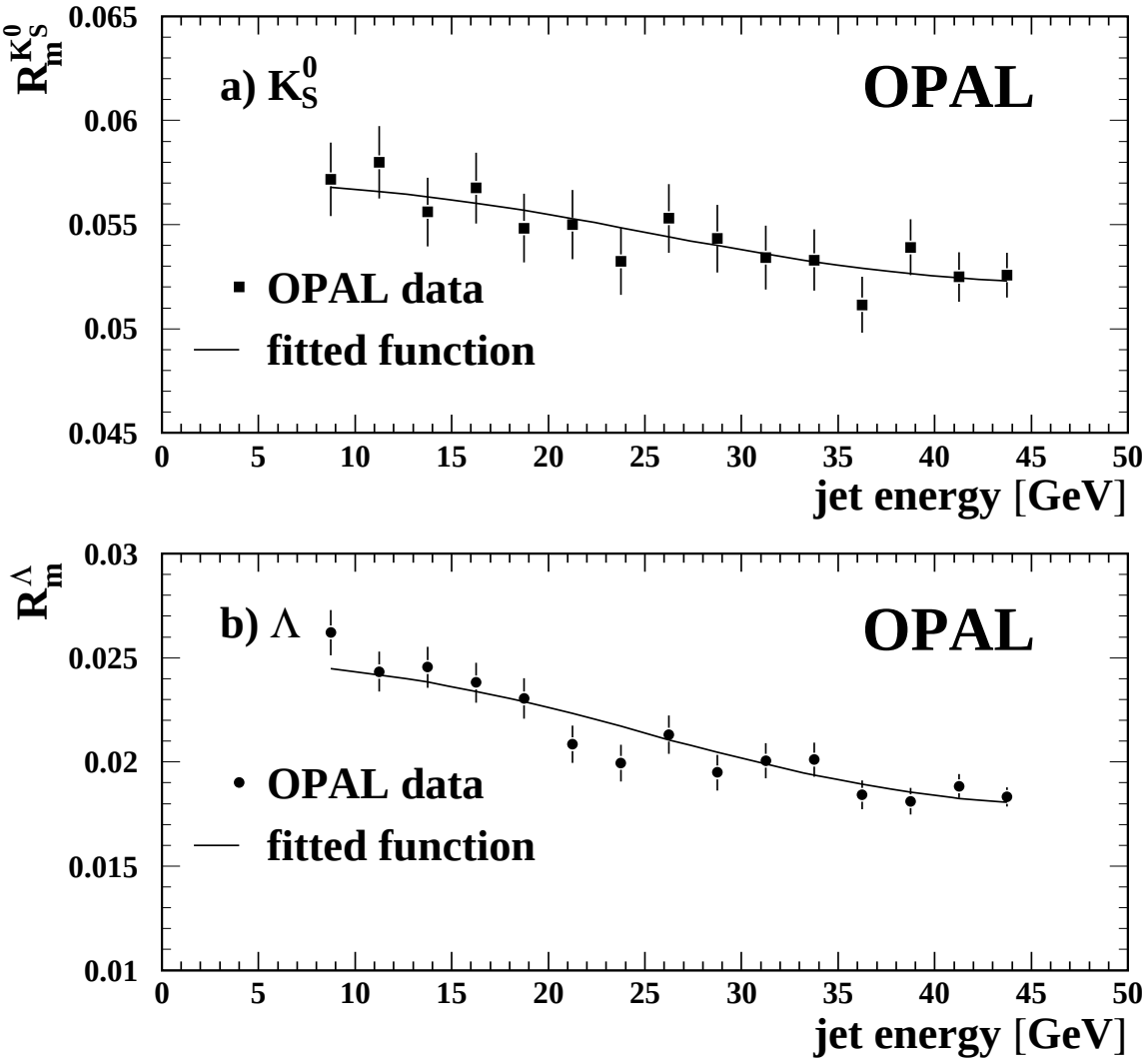

Figure 5: Relative production rates of (a) K^0_S and (b) Λ from the $y_{\rm cut}$ selection as a function of the jet energy. The lines show the functions returned from the fits of equation 1 to the data. The zeros of the vertical axes have been suppressed, and the errors shown include both statistical and systematic uncertainties.

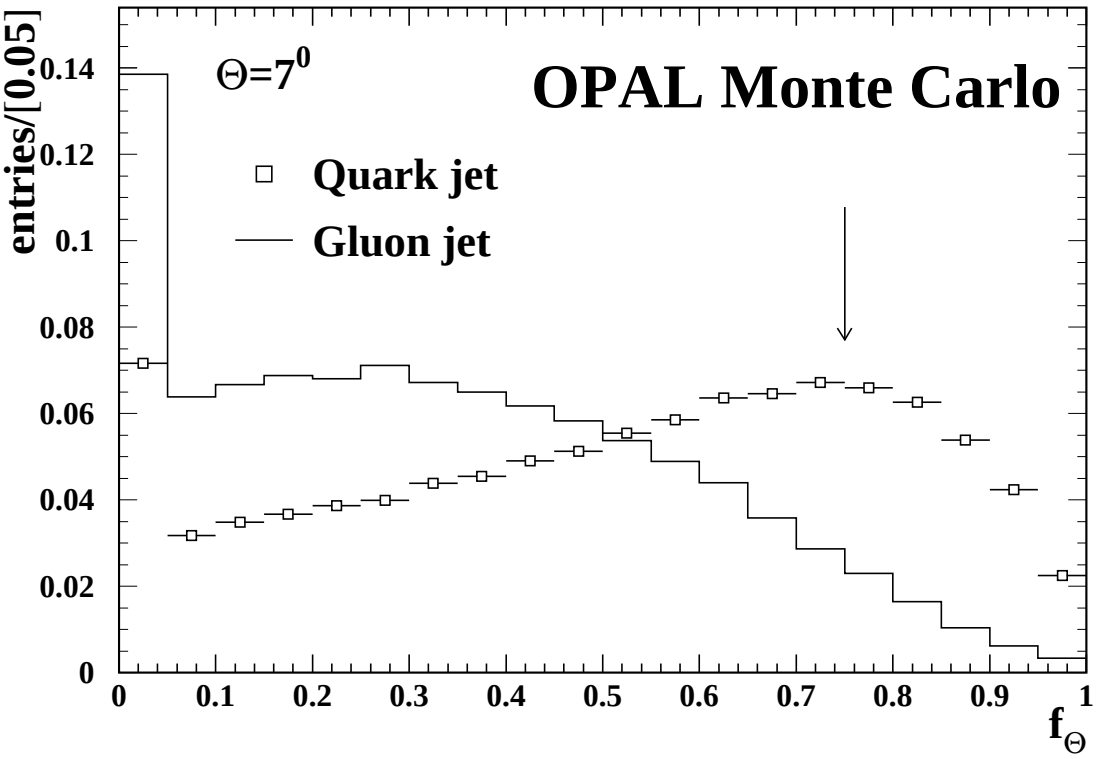

Figure 6: Distributions of f_Θ for quark and gluon jets. The events were generated with the JETSET Monte Carlo and include full simulation of the detector. The arrow indicates the cut position for selecting quark jets.

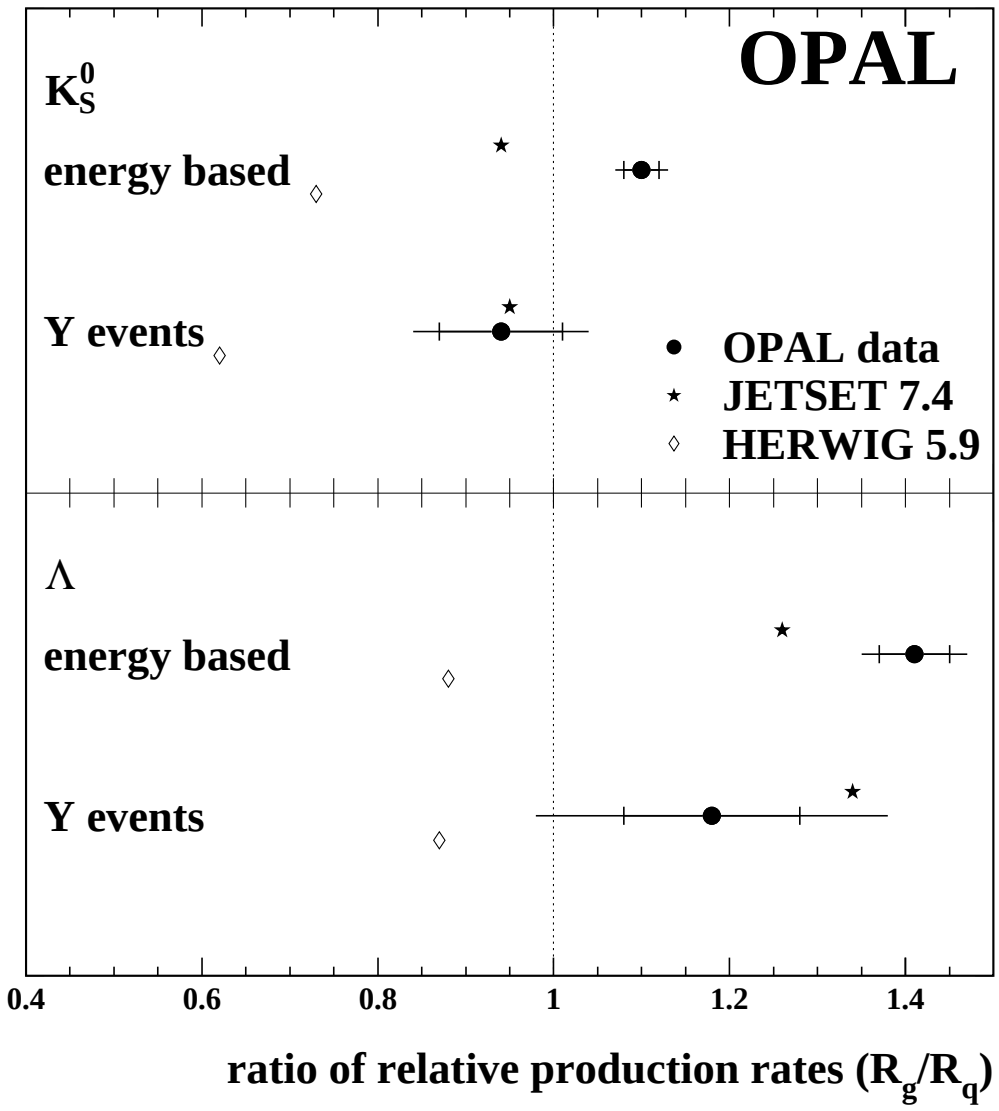

Figure 7: The ratio of relative production rates (see text) in quark and gluon jets of K^0_S and Λ for both analyses. The experimental statistical errors are delimited by the small vertical bars. The predictions of JETSET 7.4 and HERWIG 5.9 are also shown. The predictions of JETSET 7.3 are no more than 0.04 lower than those of JETSET 7.4.